Selective Photoantisepsis

David M. Harris, PhD[1] and Lou Reinisch, PhD[2]

[1] Biomedical Consultants & Associates, Inc., Paradise, California
[2] Academic Affairs, New York Institute of Technology, Old Westbury, New York

Address correspondence:
David M Harris, PhD
436 Green Oaks Drive
Paradise CA 95969
TEL: (510) 502-3345
FAX: (510) 372-0326
email: bmcinc@comcast.net

ABSTRACT

Background and Objective: Selective killing of pathogens by laser is possible due to the difference in absorption of photon energy by pathogens and host tissues. The optical properties of pathogenic microorganisms are used along with the known optical properties of soft tissues in calculations of the laser-induced thermal response of pathogen colonies embedded in a tissue model. The objective is to define the laser parameters that optimize pathogen destruction and depth of the bactericidal effect.
Materials and Methods. The virtual periodontium is a computational model of the optical and time-dependent thermal properties of infected periodontal tissues [1,2]. The model simulates the periodontal procedure: Laser Sulcular Debridement [fn1]. Virtual pathogen colonies are placed at different depths in the virtual periodontium to determine the depth for effective bactericidal effects given various laser parameters (wavelength, peak power, pulse duration, scan rate, fluence rate) and differences in pathogen sensitivities.
Results. Accumulated background heat from multiple passes increases the depth of the bactericidal effect. In visible and near-IR wavelengths the large difference in absorption between normal soft tissue and *Porphyromonas gingivalis* (*Pg*) and *Prevotella intermedia* (*Pi*) results in selective destruction. Diode laser (810nm) efficacy and depth of the bactericidal effect are variable and dependent on hemin availability. Both pulsed-Nd:YAG and the 810 nm diode lasers achieve a 2-3mm deep kill zone for pigmented *Pg* and *Pi* in soft tissue without surface damage (selective photoantisepsis). The model predicts no selectivity for the Er:YAG laser (2940 nm). Depth of the bactericidal effect is highly dependent on pathogen absorption coefficient. Highly sensitive pathogens may be destroyed as deep as 5-6mm in soft tissue. Short pulse durations enable confinement of the thermal event to the target. Temporal selectivity is achieved by adjusting pulse duration based on target size.
Conclusion. The scatter-limited phototherapy model of the infected periodontium is applied to develop a proper dosimetry for selective photoantisepsis. Dosimetry planning is essential to the development of a new treatment modality.

Key words: Dental laser, tissue model, periodontal pathogens, scatter-limited phototherapy, bacterial reduction, *Porphyromonas gingivalis, Prevotella intermedia*.

INTRODUCTION

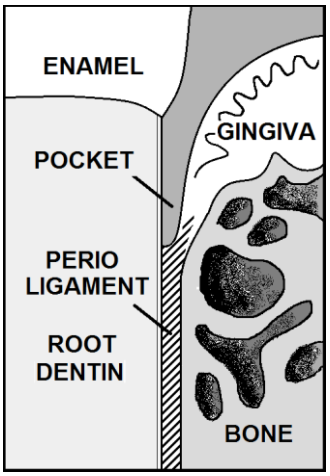

Fig. 1. The attachment apparatus is composed of the outer layer of root dentin (cementum), the periodontal ligament and alveolar bone. In this diagram the disease has caused the bone and attachment level to recede, forming a periodontal pocket.

Inflammatory periodontal disease is one of humankind's most widespread afflictions. This condition accounts for most loss of dentition in old age and chronic oral infections have been linked to several systemic conditions including pulmonary and cardiovascular disease and to pre-term, low birth weight babies [3-7].

At a cellular level the pathogens colonize the periodontal sulcus, the groove where the gingiva meets the tooth. At the base of the sulcus is the most coronal extent of the attachment apparatus that secures the tooth to the bone. This structure is composed of the alveolar bone, periodontal ligament (PL) and the outer layer of root dentin, the cementum (Fig. 1). In a healthy tooth the junctional epithelium at the bottom of the sulcus prevents oral flora from invading the body.

Most species of pathogens implicated in periodontal disease already exist in the oral cavity fluids and the natural biofilms that coat all surfaces of the oral cavity. The growth of dental plaque, gingiva irritants, trauma, smoking or other insults to the attachment apparatus will allow access for these opportunistic pathogens to colonize subgingival locations. Here they form mixed-species colonies [8,9] that assault and destroy the tissues that anchor the teeth to the bone [10]. These colonies steadily excavate a pocket (Fig. 1) that grows apically [11] until eventually the tooth is lost. Most of the infection exists within 300 microns of the surface [10-13]. However, pathogenic species such as *Porphyromonas gingivalis* (*Pg*) and *Prevetella intermedia* (*Pi*) are known to colonize areas of immunologic sanctuary such as in the cytoplasm of host cells [14-16]. These sites can be located 1 mm or more below the surface. [17,18]

Current treatment approaches include debridement of root surfaces with a surgical, mechanical and chemical armamentarium, and antisepsis of the periodontal pocket with a variety of systemic and local antibiotics. The use of intense light energy to selectively destroy the infection is another option having unique consequences. There is substantial evidence that laser treatments for infectious periodontal disease reduce the bacterial load in the periodontal pocket [19-24]. However, in clinical practice the antiseptic qualities of laser treatment are noted only as an uncontrolled consequence of the laser treatment. Arany (2016) [25] refers to this as the "bystander effect." Undoubtably, laser antisepsis can be more effective if understood in more detail and applied proactively. The technique has been successfully applied clinically for the selective removal of first degree enamel caries [26] and for the treatment of onychomycosis [27], (FDA 510(k) K943693 and K083616) [fn1 fn2]. If bacterial reduction is the primary clinical outcome of a periodontal treatment, then the optical properties of the pathogens and host tissues need to be defined. A purpose of this work is to provide a rational basis to develop a controlled clinical dosimetry.

Selective photoantisepsis is a potent laser-based modality for bacterial reduction that exploits the wavelength-specific difference in absorption characteristics between a pathogen colony and the host tissue. Photon energy is selectively absorbed by the pathogen creating a localized, rapid and lethal increase in temperature. To develop an accurate clinical dosimetry we need to know: (1) What is the sensitivity of the specific pathogens to laser light relative to the surrounding tissues, (2) How deep into

the tissue does the selective bactericidal effect actually reach during a laser procedure and (3) Can dosimetry be adjusted to optimize the depth of bactericidal effect without surface damage?"

To address these questions we apply scatter-limited phototherapy, [1] a computational tissue model that predicts the magnitude and distribution of the thermal response of tissue to laser irradiation. It is based on the Beer-Lambert Law and the known optical and thermal properties of different tissue components (mucosa, connective tissue, bone, dentin, etc.). The addition of the tissue heat capacity and thermal diffusion then predicts the temperature distribution in space and time during the course of a laser treatment procedure. [2] Temperature contours identify the spatial distribution of important tissue effects such as coagulation at 60^{o}C and vaporization at 100^{o}C.

We have studied the interaction of laser energy (1064nm and 810nm) with periodontal pathogens in culture [28-31] and have measured the absorption spectra of *Pg* and *Pi* from 400-1100nm [32]. These measurements of the optical properties of specific pathogens incorporated into the model allow us to define the appropriate dosimetry for selective photoantisepsis and to optimize the parameters to lethally treat those pathogens. Near-real time simulations presented as videos provide a medium to communicate these empirical findings into a clinically meaningful format.

METHODS

<u>The virtual periodontium: A computational model of the infected periodontium</u>.
The details of the scatter-limited phototherapy model have been described in detail in previous publications. [1,2] We chose to use this model because the speed of the calculations allows one to make a time series of evaluations. Time dependent temperature profiles of tissue during and after laser irradiation are extremely valuable in understanding laser therapy.

The scatter-limited phototherapy model uses measured tissue parameters for absorption, scatter, thermal conductivity and heat capacity to make these calculations. By recognizing that light is distributed with a Gaussian distribution in homogeneous tissue, we can avoid having to solve inhomogeneous partial differential equations. Thus, the profiles can be rapidly generated and profiles as a function of time can be sequenced to create videos. The videos demonstrate the changing thermal gradients inside the tissue during a laser procedure.

Since the model uses only measured parameters, it is not a surprise that predictions of thermal damage from the model agree with the actual measurements of thermal damage. We have shown this correlation between measured thermal damage and predictions in the infrared at 1064 nm and 10.6 μm [1] and visible at 532 nm [2].

Figure 2 is a modification of the algorithm previously developed [2] with the substitution of pathogen colonies for the vasculature used in that study. The soft tissue in the current model is the PL. Fourier Transforms are used to convolve three different calculations. The delivery geometry of the laser beam and the pulse structure and energy per pulse are used along with the tissue scattering and absorption characteristics to determine the distribution of photons in the tissue. The photon distribution is changed to a temperature distribution by factoring in the heat capacity. Thermal diffusion then determines the space/time dissipation of the temperature distribution. If there are multiple pulses the process is repeated starting with the existing temperature distribution. These simulations incorporate the changing conditions during a laser surgical procedure caused by movement of the fiber. The

parameter "velocity" determines the location of subsequent pulses, that is, the speed of the laser beam as it is scanned over the tissue.

Fig. 2. Flow chart of the computational model used to determine the thermal distribution in tissue during laser irradiation.

The insert shows the cylindrical geometry of the periodontal ligament (PL). When showing the thermal gradients we open and flatten this cylinder to a flat rectangle.

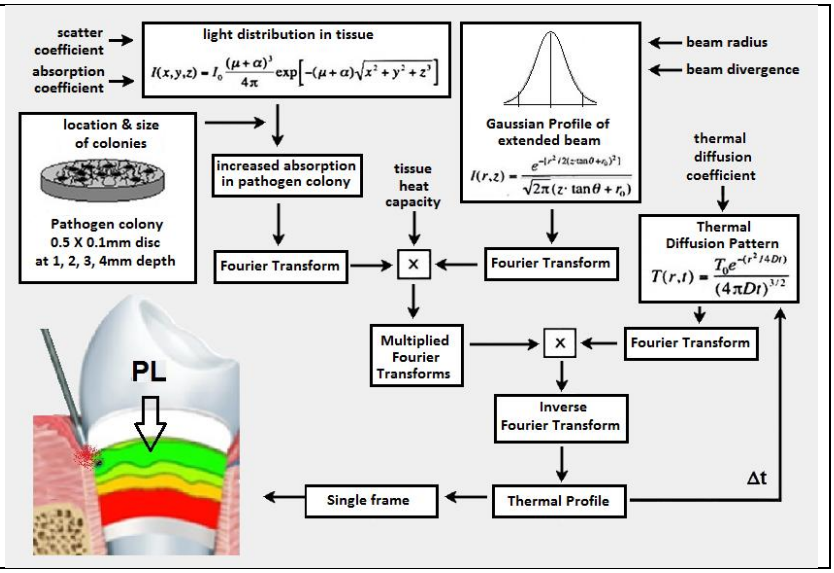

In previous work on scatter-limited phototherapy it was determined that the spread of light in quasi-homogeneous tissue could be approximated with a Gaussian distribution [1,2]. The amount of scattering is normally written with a reduced scattering coefficient, μ_s, such that

$$I(x,y,z) = I_0 \frac{\mu_s^3}{4\pi} \exp\left[-\mu_s\sqrt{x^2+y^2+z^2}\right] \qquad (1)$$

where I(x,y,z) is the 3-dimensional distribution of light in the tissue and *z* is the coordinate axis into the thickness of the tissue.

In addition to the scatter presented in Eq. (1), absorption will limit the penetration of the light in the tissue. Beer's Law is used to describe the absorption in isotropic three dimensions

$$I(x,y,z) = I_0 \frac{\mu_a^3}{4\pi} \exp\left[-\mu_a\sqrt{x^2+y^2+z^2}\right] \qquad (2)$$

Equations (1) and (2) can be combined to give the spread of light in any scattering and absorbing medium, such as skin, gingiva or ligament. These combine to

$$I(x,y,z) = I_0 \frac{(\mu_s+\mu_a)^3}{4\pi} \exp\left[-(\mu_s+\mu_a)\sqrt{x^2+y^2+z^2}\right] \qquad (3)$$

Note that scattering and absorption behave much the same way; both scattering and absorption limit the penetration of light. Using these known functions to describe the spread of the light, one does not need to use a Monte Carlo simulation and the calculations take much less computational time than a Monte Carlo simulation.

Anatomy of the virtual periodontium.

The model created for this work is stylized to a standard tooth. The tooth root is cylindrical and just under 2.0 cm in circumference (about 6 mm in diameter). The root is completely surrounded by the attachment apparatus. The tissue is assumed homogeneous, except for the implanted bacterial cultures, and is 1.0 cm deep and the thickness is at least 1 mm. For these simulations the laser fiber is in the pocket (Fig. 1) and is perpendicular to and in contact with the upper surface of the PL. The output of the laser is through a 360 micron diameter optical fiber which is scanned 20 mm around the circumference of the root in the periodontal pocket (or scanned across the top of the flattened surface). In our simulations, we unroll the cylinder of PL and lay it flat. So the cylinder is a flat rectangle. Irradiation variables include: wavelength, spot size (determined by the fiber diameter and distance from the surface), angle of the fiber relative to the surface, average power, pulse duration, peak power, energy per pulse, repetition rate, scan velocity and number of passes.

Simulations are made on 1.0 cm x 2.0 cm pieces of virtual tissue with 0.005 cm (50μm) resolution. Thus, the virtual tissue comprised 80,000 pixels. All simulations were checked by doing a test simulation at a single time point with 0.001 cm (10 μm) resolution (2,000,000 pixels) to confirm reproducibility and to demonstrate that 0.005 cm was sufficient resolution. Spatial resolution was set at 0.0005 cm (5 μm) to examine effects of pathogen size in SIM 4.

Virtual pathogen colonies are placed at various depths so the bactericidal effectiveness can be determined from the temperature increase. Colony size is examined in simulation #4. Otherwise, colonies are 0.5mm diameter, 0.1 mm thick discs with a volume of 0.2 mm^3 (Fig. 2). Since the PL is well vascularized we assume the bacteria, *Pg* and *Pi*, are pigmented *in vivo* and use absorption coefficients: μ_{aPg} = 10 cm^{-1} at 810nm, 7.7 cm^{-1} at 1064nm [26] and 13,000 cm^{-1} at 2940nm [33]. Data are also available at 1064nm for several fungal pathogens, including *Candida albicans* (*Ca*, μ_{aCa} = 75cm^{-1}), and *Scytalidium dimidiatum* (*Sc,* μ_{aSc} = 375 cm^{-1}) [34].

This highly accurate and predictive mathematical model is applied to simulate selective photoantisepsis of periodontal pathogens during laser sulcular debridement. The beam shape and fiber-optic mode of delivery are those typically used for the procedure. Zones of potential tissue damage (60^{o}C) and vaporization (100^{o}C) are identified with the model. The location and magnitude of these thermal contours are used to predict pathogen destruction.

The current model of the infected periodontium is composed of pathogen colonies embedded in the PL. The periodontal ligament is a dense fibrous connective tissue composed of collagen, ground substance, vascular and neural networks, other cells and water [35]. Most of these components add very little to absorption at the wavelengths of 810nm and 1064nm. The absorption of light by the PL is, thus, predominately a mixture of the absorption of light by water and by hemoglobin. Foong and Sims (36) report that the microvascular volume of the periodontal ligament in humans ranges from 1.63% to 3.5%. Estimates of the water volume of ligament is about 75% (37) although exact values for periodontal ligament are not currently available. The absorption of light by water is well understood and the absorption coefficients as a function of wavelength can be obtained from the publication by Hale and Querry [38]. The absorption of light by hemoglobin can be due to oxy hemoglobin (HbO_2) or deoxy hemoglobin (Hb). The molar extinction coefficients as reported by Zijlstra et al. [39] are used for the absorption in healthy soft tissue due to Hb and HbO_2. The PL is modeled as normal soft tissue at 75% water and blood volume 1.7% (35 μM HbO_2 and 60 μM Hb). This is plotted in Fig. 3 along with absorption spectra for the darkly pigmented periodontal pathogens *Pg* and *Pi* [32] and pure water.

Figure 3. Absorption spectra from 500-1100nm for the periodontal pathogens *Pg* and *Pi,* [28] soft tissue (PL) and water. There are orders of magnitude differences in relative absorption between the bacteria and the host tissues at both 810nm and 1064nm.

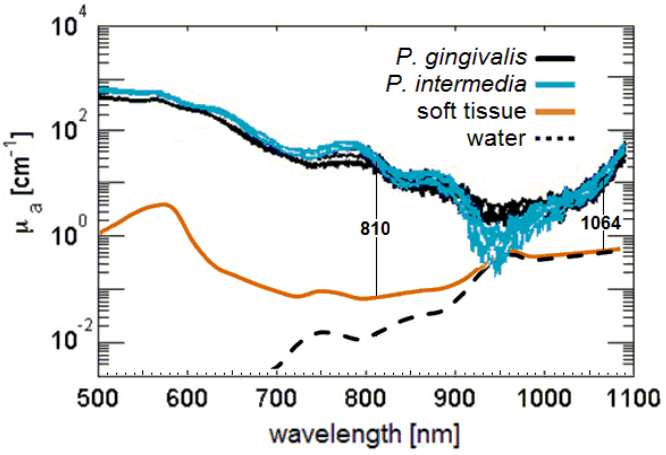

After we calculate how the light is distributed in the tissue, we then converted that light energy into a temperature increase using the heat capacity of soft tissue, 3.7 J/gK. The thermal energy is not fixed into the tissue, but it will dissipate or thermally diffuse. The thermal diffusion is modeled with:

$$T(x,y,z,t) = T_{\max} \frac{1}{(4\rho Dt)^{3/2}} Exp\left[\frac{(x^2+y^2+z^2)}{4Dt} \right] \quad (4)$$

In Eq. (4), *T* is temperature, *t* is time and *D* is the thermal diffusion coefficient. We can write $D = k/\rho c_p$, where k is the thermal conductivity, ⍰ is the density and c_p is the specific heat capacity. This allows us to independently calculate *D* for a well-known substance, like water (*D* = 0.0014 cm^2/s). We use *D* = 0.0023 cm^2/s for the tissue. This comes from measurements of thermal damage as a function of laser pulse length [1,40] and is close to the value of water.

In the simulations, we typically use the laser pulse length as the shortest time step. If each simulation were used as a video frame, the movies would appear as very slow-motion movies and all movies would run at different rates. So, we take every nth frame so that there are equal time steps of 0.025 s between the movie frames (or 40 frames is 1.0 s of time duration in the animation). For instance, if we have a 1.0 ms laser pulse, then 1.0 ms becomes the time resolution. However we only use one frame every 25 frames to make the movie. Depending on the computer and the video format, the movies run at about ½ of real time. The laser scanning over 20 mm should take 2 s, but the movies require roughly 4 s.

The damage zones are shown where the temperature exceeds 60˚C (aqua color) and where the temperature exceeds 100˚C (pink color). Even though the tissue or bacterium might reach 100˚C, they do not necessarily ablate or vaporize. To change the water from liquid water to steam, the latent heat of vaporization must be added to the target in addition to enough heat to bring the temperature up to 100˚C. Only with the Er:YAG laser does the tissue receive a sufficient amount of heat and actually ablate. With the Nd:YAG and diode lasers in these simulations, the tissue only reaches 100˚C but seldom vaporizes.

Four sets of simulations were calculated for this study: SIM 1 looked at the three lasers commonly used for laser sulcular debridement: the 810 nm diode laser, the 1064 nm Nd:YAG laser and 2940 nm Er:YAG

laser. The 810 nm diode laser was delivered in 1 ms pulses, 6 mJ per pulse and repeated at 500 Hz repetition rate. The average power of the diode laser with these parameters would be 3 W. The Nd:YAG laser at 1064 nm was delivered in 150 µs pulses, 200 mJ per pulse and repeated at 20 Hz repetition rate. The average power of the Nd:YAG laser with these parameters would be 4 W. The Er:YAG laser at 2940 nm was delivered in 150 µs pulses, 100 mJ per pulse and repeated at 20 Hz. The average power of the Er:YAG laser with these parameters would be 2 W. In these simulations, the bacterial absorption coefficients were 10 cm^{-1} at 810 nm, 7.7 cm^{-1} at 1064 nm [32] and 13,000 cm^{-1} at 2940 nm [33].

SIM 2 looked at the 810 nm diode laser being applied at an average of 2, 3, 4 and 5 W. At all power levels the pulses were 1 ms in duration and repeated at 500 Hz. The energy per pulse was set at 4 mJ, 6 mJ, 8 mJ and 10 mJ to achieve the different average power levels. In these simulations the bacterial absorption coefficients were 10 cm^{-1}. The video shows only the simulations at 4, 6 and 8 mJ/pulse.

SIM 3 looked at the Nd:YAG laser with three different bacterial colonies, each having distinctly different absorption coefficients at 1064 nm. The three bacteria were, *Pg* with an absorption coefficient of 7.7 cm^{-1} at 1064 nm, *Ca* with an absorption coefficient of 75 cm^{-1} at 1064 nm and *Sc* with an absorption coefficient of 375 cm^{-1} at 1064 nm.

SIM 4 explored the thermal confinement as a function of the pulse duration. Since the thermal confinement is closely related to the target size, two different size bacterial colonies were used. In this simulation, the pulse durations of the Nd:YAG laser at 1064 nm were stepped by factors of 10 from 15 µs to 15 s. The bacterial colonies were 500 µm and 50 µm in diameter. The absorption coefficient of the bacterial colonies was 7.7 cm^{-1}.

RESULTS

Fig. 4. Understanding the videos. The anatomical location of the simulations is the PL, (Fig. 2) which is unrolled and laid flat as shown in the three panels. Each panel represents the thermal response to a different dental laser:
Diode: 810nm; 1 ms, 6 mJ/pulse, 500 Hz.
Nd:YAG: 1064nm; 150 μs, 200 mJ /pulse, 20 Hz.
Er:YAG: 2940 nm; 150 μs, 100 mJ/pulse, 20 Hz.
The three panels are single frames (snap shots) from SIM1, the 3-wavelength video. During the video, the optical fiber (green vertical bar) delivering the laser makes four scans across the top of the tissue with a constant speed. The color contours illustrate the dynamic thermal response of the soft tissues and pathogen colonies. In all three panels the scan rate of the optical fiber is 1 cm/s. Pigmented *Pg* discs are located at 1, 2, 3 and 4 mm below the surface and are shown in the figure.

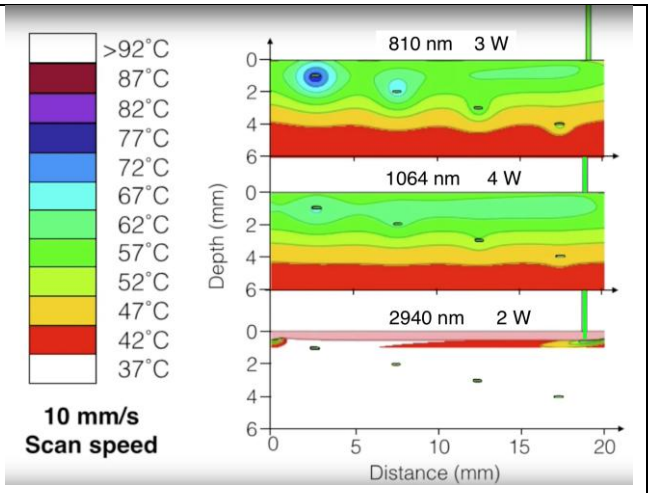

Data presentation (Fig. 4).
A single frame from the SIM 1 video is shown in Fig. 4. The videos illustrate the evolving temperature profiles in the PL. The fiber is positioned perpendicular to the PL surface and moves at a constant rate around the tooth four (4) times (or across the top of the flatten geometry shown in Fig. 4). Color contours represent 5°C increments. Ambient (white background) is 37°C, light blue is 62°C, and white is > 92°C. Damage zones are shown at the end of each video and also in Fig. 5. These plots represent the areas that reached 60°C and 100°C at some time during the four passes.

[The simulations are the results of this study. View SIM 1 video here]
http://biomedicalconsultants.pub/wavelength/

SIM 1. Three Dental Laser Wavelengths.
Three commonly used lasers in dentistry are tested on the virtual periodontium: a diode laser emitting at 810nm, a pulsed Nd:YAG laser at 1064 nm, and a similar pulsed Er:YAG laser at 2940 nm. The typical 6 W diode laser output can be pulsed on and off with an electronic shutter. The peak power of a gated pulse is constant for any pulse duration and, thus, shorter duration pulses contain less energy. For this example, a 1 ms pulse with a peak power of 6 W will only contain 6 mJ of energy. In order to achieve 3 W of average power the diode laser must deliver 500 6 mJ pulses per second (500Hz). In contrast, the pulsed Nd:YAG and Er:YAG lasers can achieve very high peak powers with very short duration pulses. In this case, Nd:YAG and Er:YAG pulses are set at 150 μs duration. The Nd:YAG pulse contains 200 mJ of energy delivered at 20 Hz (4 W average and 1333 W peak powers). The Er:YAG power is limited by fiber transmission to 100 mJ, 20 Hz (2 W average and 667 W peak power).

For SIM1 the laser parameters at 810 nm and 1064 nm have been adjusted to maximize *Pg* destruction to a depth of 2 mm without surface damage. One can observe the accumulation of background heat with each pass over the tissue. As a result deeper colonies are affected as the ambient temperature

increases with each pass. It is observed that the diode and Nd:YAG lasers completely destroy the 1mm colonies on first pass and the 2 mm colony by the fourth pass.

At the end of SIM1 and in Fig. 5A the blue zones represent areas that reached 60° C and pink areas reached 100° C by the end of the simulation. The short 150 μs pulses of the Nd:YAG laser demonstrate greater confinement of thermal damage to the target than the 1 ms pulses from the diode laser. The concept of selective photoantisepsis is well visualized in the video as "hot spots" within a much colder surround that appear where the bacterial colonies are (were) located.

The bottom Er:YAG laser panel shows selective removal of the soft tissue surface with very little deep collateral damage. The 2940 nm wavelength of the Er:YAG laser is highly absorbed by water (μ_α = 13,000 cm^{-1}) and, thus, has a much shallower penetration depth than the diode or the Nd:YAG. Consequently, photons are absorbed at the surface and insufficient energy reaches the buried colonies. High absorption by water means explosive vaporization of the surface [41,42]. Also, there is no differential absorption since the pathogens and the surrounding tissues are both mostly water. Our simulations indicate that the Er:YAG wavelength will provide efficient surface disinfection; [43-47] however, simulations at this wavelength predict no selective photoantisepsis.

[View SIM 2 video here]
http://biomedicalconsultants.pub/power-diode/

SIM 2. Power series with the810nm diode laser.
Fig. 5B shows the damage zones resulting from 4 passes with an 810 nm diode laser with 1 ms gated pulses delivered at a rate of 500Hz. The fiber velocity is 1 cm/s. At 810 nm the 3W condition is optimal for selective destruction of *Pg* colonies down to 2 mm with other parameters remaining constant. Increasing power to 4 W increases depth of bacterial damage to 3 mm, but now the simulation predicts potential surface damage. In this example the bactericidal zone extends 1-2 mm below an undamaged surface or 1-2 mm beyond the margin of coagulated tissue. The simulation assumes darkly pigmented bacteria. At this wavelength less pigment in the bacteria will result in lower absorption [32].

[View SIM 3 video here]
http://biomedicalconsultants.pub/pathogen-abs/

SIM 3. Pathogen absorption coefficient - influence on depth of pathogen damage.
There is considerable variance in the absorption characteristics of the myriad of pathogens that invade our tissues. SIM 3 illustrates how pathogen absorption has a significant effect on the depth of damage (Fig. 5C). *Pg* and *Pi* demonstrate only moderate absorption at 1064 nm (μ_{aPg} = 7.7 cm^{-1}) compared to other pathogens tested. *Ca* is more sensitive with an ablation threshold of 5 J/cm^2 and an absorption coefficient, μ_{aCa} = 75 cm^{-1}. SIM 4 shows that the *Ca* colony can be destroyed down to 3-4 mm without surface damage. For a very sensitive pathogen with an μ_a = 375 cm^{-1} (e.g., *Aspergillus fumigatus* and *Scytalidium dimidiatum*) a 1 mm deep colony will vaporize on the first pass (not shown) so in the bottom panel pathogen colonies are moved to 3, 4, 5 and 6 mm. With these laser parameters the *Sc* colony at 5mm is totally destroyed and even the 6 mm deep colony is damaged.

A 5-6 mm depth of damage is demonstrated for non-periodontal pathogens. These values may also apply to certain other periodontopathogens. [48]

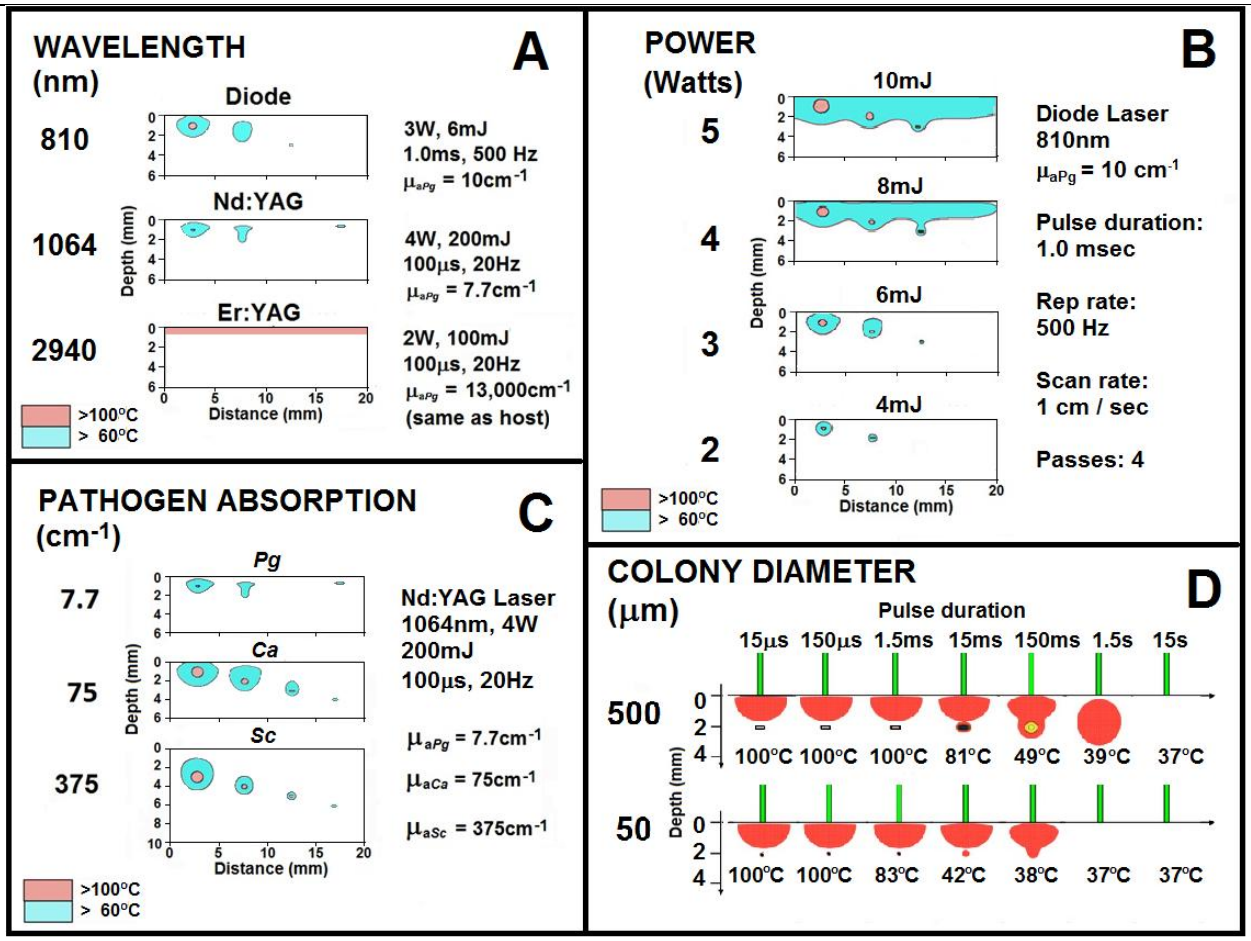

Fig. 5. Damage zones achieved during the simulations.

A. Different wavelengths damage zones from SIM1. The contours represent the temperatures achieved by the end of Pass 4. Blue = possible damage based on exposure duration; Pink = definite damage. The diode and Nd:YAG parameters have been optimized for selective destruction of pigmented *Pg* colonies. The Er:YAG demonstrates no selectivity.

B. SIM 2 is an 810nm diode laser where average power level is varied from 2W to 4W. Shown here are the damage zones following 4 passes at a series of power levels that include an additional panel for the 5W response. The 3W panel is the optimized response shown in A. Increasing power level to 4W increases depth of pathogen damage from 2mm to 3mm but this also causes potential surface damage.

C. The effect of pathogen absorption coefficient is examined in SIM 3. Identical laser parameters are applied in all three conditions. Shown are damage zones for three different pathogen species with different sensitivities to the 1064nm wavelength. Under these conditions *Pg* is destroyed down to 1-2mm, *Ca* to 3-4mm and *Sc* as deep as 5-6mm.

D. Colony size determines thermal relaxation time. In this simulation a single pathogen colony (μ_a = 75 cm^{-1}) is positioned in the beam path 2mm below the surface. The fiber is stationary and a single 200mJ, 1064nm pulse of variable duration is delivered. Each row is a different colony diameter. The temperature achieved in the center of each colony is listed. The red contour is 42°C. Higher temperature contours were attained but are too small to show in the figure. Because the smaller target dissipates heat more rapidly it requires a shorter duration exposure to achieve thermal damage.

SIM 4. Pulse duration - Temporal selectivity based on target size (no video)

A short duration pulse from the Nd:YAG laser provides confinement of thermal damage to the pathogen colony. In SIM 5 (Fig. 5D) in a single pulse a constant amount of energy (200 mJ) is delivered over a variable duration so that peak power decreases as pulse duration increases. In a small target heat may be dissipated as rapidly as it accumulates and with long duration exposures it will reach an equilibrium temperature below damage threshold. A longer duration pulse allows more time for heat to spread to surrounding tissues and creates a larger zone of collateral damage. Exposures for very long durations with very low peak powers have virtually no effect.

This simulation provides an example of temporal selectivity. The pulse duration must be short enough to affect small targets [49]. Figure 5D shows for the parameter set tested that a typical colony size of 50μm requires a pulse at least as short as 150 μs to achieve 100°C. A longer duration 1.5 ms pulse will only reach 83°C. Calculations indicate that an even smaller 5 μm pathogen cluster will require a 15 μs or shorter pulse. And, in order to be lethal to a lone 1-μm spherical pathogen (e.g., [12,50]) the 200 mJ pulse needs to be delivered in less than 1 μs!

Thermal confinement and selective destruction from selective absorption and short pulses.
One influence on selectivity is the differential absorption between bacteria and normal tissue. Both 810nm and 1064 nm wavelengths demonstrated this selectivity. Given the assumptions of the model we estimate a bactericidal zone that extends up to 6mm below an undamaged surface. If the laser procedure produces an ablated or coagulated surface then the bactericidal zone moves deeper into the tissue beyond the zone of coagulation.

There appears to be potential for high selectivity at 810 nm (Fig. 3). This wavelength will also target hemoglobin within the vasculature so the selectivity will be a result of the pathogen/surround concentration difference in hemin. We have modeled normal connective tissue, whereas, the pathogens often reside in inflamed tissue with a higher blood volume. Soft tissue background absorption at 810nm will be higher in the presence of inflammation. Although pathogens are modeled as if darkly pigmented, there must also be sufficient hemin availability *in vivo* to sensitize the pathogens. These factors will all influence estimates of selectivity at 810 nm. The efficacy of the 1064 nm wavelength appears to be independent of blood volume or pigmentation [32]. However, at any wavelength the efficacy of pathogen destruction is highly dependent on the absorption coefficient of the pathogen at that wavelength (Fig. 5C).

Another influence on selectivity is the thermal confinement achieved with high peak powers and short pulse durations [51]. Since it requires time for heat to dissipate into the surrounding tissues, a short duration pulse will limit this spread resulting in less collateral damage. The videos illustrated how the heat energy is initially concentrated at the surface, as well as in the buried pathogen colonies, and then dissipates into the surround. The volume of the tissue heated is important in calculations of heat dissipation. Different sized pathogen colonies will have different thermal relaxation times.

The heat may have relaxed from the colony in a short time, while the larger volume of normal tissue heated by the laser takes much longer to cool down. Even at low repetition rates (e.g, 2 Hz) calculations show that the surrounding tissue does not completely cool down between laser pulses [2]. Note that the definition of thermal relaxation time [49] is not the time to return to equilibrium but the time required to decrease by one-half from the maximum temperature. As a result, the tissues surrounding the pathogen colonies accumulate heat. Because of this continuous increase in ambient temperature during a laser procedure the deeper colonies can be destroyed with subsequent passes. For example in

SIM2/3W the 1mm colony is destroyed on the first pass but the 2mm colony is not destroyed until the fourth pass.

Irreversible thermal damage can be described for biomolecules like collagen, [52] but what constitutes destruction for an entire pathogen colony is less certain. Vaporization clearly means destruction. We assume pathogen death occurs within the 100^{o}C contours in the simulations (although actual vaporization may not occur until higher temperatures). There is also a zone of cell death beyond this area where biomolecules that are essential to life have been irreversibly denatured (coagulated). For long duration exposures this zone may extend as far as the 60^{o}C contours in the simulations. The extent of this damage zone is determined by several factors. The simulations illustrate how wavelength, scan speed, number of passes, power level, pulse duration, the absorption coefficient of the target pathogen and the differential absorption between pathogen and host tissue all can affect the amount of collateral damage and the "depth of kill."

Summary of the simulations.
It is evident how the tissue responses and efficacy can be quite different for the three commonly used dental lasers. The real-time videos clearly illustrate selective destruction of pathogen colonies several millimeters below an undamaged surface at both 810 nm and 1064 nm. Based on our measurements and calculations we predict that *Pg* and *Pi* can be damaged to a depth of 2-3 mm using appropriate laser parameters. This zone of antisepsis remains 1-2mm beyond the zone of laser-coagulated tissues. Some pathogens that are highly sensitive to 1064nm light can be destroyed up to 5-6 mm into soft tissue. Short duration pulses provide thermal confinement to the target and are required to be effective against very small targets.

DISCUSSION

Simulations versus reality.
We have simulated the periodontal surgical procedure, laser sulcular debridement, to gain a more detailed understanding of dosimetry for selective photoantisepsis. The conditions have been simplified in order to explore the basic concepts. As a result, the simulations are idealized relative to real-life laser surgery.

In common practice the light energy from an 810 nm diode laser is converted into heat at the distal tip of the fiber by "initiating the tip," that is, collecting light absorbing debris on the tip [53]. During laser sulcular debridement with the pulsed Nd:YAG or Er:YAG, charred and coagulated tissues also accumulate on the fiber tip. These effects are not included in the calculations. The simulated motion is robotic with a constant velocity and does not accurately reflect the true motion of the surgeon's hand. The simulated shape of the periodontal pocket is symmetrical and conditions are constant, whereas the actual surgical environment is irregular and dynamic with rapidly changing conditions that require immediate clinical judgment.

Clinical utility of selective photoantisepsis. The presence of pathogenic organisms is considered to be necessary to the progression of periodontitis. *Pg* and *Pi* have been established as pathogenic bacteria involved in the periodontal disease process. [54-59]. *Pg* and *Pi* are pigmented, gram-negative, motile anaerobic bacteria known to cause tissue destruction by release of proteinases [60-62] and lipopolysaccharides [63-65]. They are known to adhere to and enter epithelial cells [4,15,54,66-69]. Intracellular bacteria can evade host immune effectors and antibiotics commonly used to treat infection. Subgingival pathogenic bacteria tend to colonize stagnant ecological niches, or privileged sites [54] such as surface irregularities that favor retention and growth [61]. They are also known to colonize calculus

and cementum, and penetrate into dentinal tubules and lacunae. [10,70,71] *Pg* is mostly concentrated attached to the biofilm surface, [12] although it has been identified migrating far as 2-mm into the dentinal tubules [10,].

These bacterial reservoirs are sources for recolonization of treated root surfaces. Since they are not eliminated by conventional mechanical treatment, it has become appropriate to combine mechanical periodontal therapy with the use of chemical antibiotics [12]. Antimicrobials may help to reduce the number of microorganisms within the periodontal pocket to levels lower than may be achieved with scaling alone but have limited access to privileged sites. Tetracycline and chlorhexadine have been shown to not penetrate much past the cemento-dentin junction [72,73] and intra-root canal antibiotic irrigates penetrate only a few 100 microns into the surrounding dentin [74]. Chemical antibiotics have additional disadvantages that include: potential allergic reactions [75], systemic side effects [76] and possible induction of drug resistance [77-83].

The laser mode of antisepsis is currently an uncontrolled consequence of many dental laser procedures. With proper dosimetry it can be developed for specific applications. Selective photoantisepsis may have several advantages over traditional antibiotics in pocket disinfection: (1) a therapeutic dose can be delivered to a greater depth immediately and leaves no residual concentration in the host or environment; (2) laser radiation affects equally extracellular and intracellular pathogens and can access other privileged sites such as calculus and dentinal tubules; (3) photoantisepsis has no known negative systemic side-effects, or interactions with other modes of therapy. The technique of selective photoantisepsis described for the periodontal pocket has potential applications in root canal antisepsis [84-86] and other medical fields [278,87,88].

CONCLUSION

Scatter-limited phototherapy is used to demonstrate that the 810 nm diode laser and the 1064 nm Nd:YAG can have a bacterical effect during laser sulcular debridement. In our simplified model, this effect could be 2 or more mm below the surface. The selective photoantisepsis of these lasers spares most of the PL and adjacent tissues while selectively destroying the pathogen colonies.

ACKNOWLEDGMENTS

We thank John Sulewski and the anonymous reviewers for their editorial assistance and thought provoking comments.

Address correspondence to: David M. Harris, PhD, bmcinc@comcast.net

FDA 510(k) Clearances cited in the text.

Fn1 K961269. American Dental Technologies, Inc. (1997). "[Laser] Sulcular debridement (removal of diseased or inflamed soft tissue in the periodontal pocket) to improve clinical indices including gingival index, gingival bleeding index, probe depth, attachment level and tooth mobility."

Fn2 K943693. Incisive Technologies, Inc. (1994). “Selective ablation of enamel (first degree) caries.”

Fn3 K083616. PathoLase, Inc. (2008). “Increase in clear nail”

REFERENCES
Literature Cited

01. Reinisch L. Scatter-limited phototherapy: A model for laser treatment of skin. Lasers in Surg Med 2002;30(5):381-388.
02. Reinisch L, Garrett CG, Courey M. A simplified laser treatment planning system: Proof of concept. Lasers Surg Med 2013; 45(10):679-685.
03. Dorn B, Dunn WA Jr, Progulske-Fox A. Invasion of human coronary artery cells by periodontal pathogens. Infect Immun 1999;67(11):5792-5798.
04. Deshpande RG, Khan M, Genco CA. Invasion strategies of the oral pathogen *Porphyromonas gingivalis*: Implications for cardiovascular disease. Invasion Metastasis 1998-1999;18(2):57-69.
05. Emingil G, Buduneli E, Aliyev A, Akilli A, Atilla G. Association between periodontal disease and acute myocardial infarction. J Periodontol 2000; 71(12):1882-1886.
06. Jeffcoat MK, Geurs NC, Reddy MS, Cliver SP, Goldenberg RL, Hauth JC. Periodontal infection and preterm birth. Results of a prospective study. J Am Dent Assoc 2001;132(7): 875-880.
07. Jeffcoat MK, Jeffcoat RL, Gladowski PA, Bramson JB, Blum JJ. Impact of periodontal therapy on general health: Evidence from insurance data for five systemic conditions. Am J Prev Med 2014;47(2):166-174.
08. Feuille F, Ebersole JL, Kesavalu L, Stepfen MJ, Holt SC. Mixed infection with *Porphyromonas gingivalis* and *Fusobacterium nucleatum* in a murine lesion model: Potential synergistic effects on virulence. Infect Immun 1996;64(6):2094-2100.
09. Grenier D. Nutritional interactions between two suspected periodontopathogens, *Treponema denticola* and *Porphyromonas gingivalis*. Infect Immun 1992;60(12):5298-5301.
10. Socransky SS, Haffajee AD. Microbial mechanisms in the pathogenesis of destructive periodontal diseases: A critical assessment. J Periodont Res 1991;26(3):195-212.
11. Rateitschak KH, Rateitschak EM, Wolf HF, Hassell TM. Periodontology (2nd ed.). Thieme Medical Publishers, Inc., New York, pp 22-27, 1989.22-24
12. Adriaens PA, Edwards CA, De Boever JA, Loesche WJ. Ultrastructural observations on bacterial invasion in cementum and radicular dentin of periodontally diseased human teeth. J Periodontol 1988;59(8):493-503.
13. Adriaens PA, De Boever JA, Loesche WJ. Bacterial invasion in root cementum and radicular dentin of periodontally diseased teeth in humans. A reservoir of periodontopathic bacteria. J Periodontol 1988; 59(4):222-30.
14. Duncan MJ, Nakao S, Skobe Z, Xie H. Interactions of *Porphyromonas gingivalis* with epithelial cells. Infect Immun 1993;61(5):2260-2265.
15. Dorn BR, Leung K-P, Progulske-Fox A. Invasion of humanoral epithelial cells by Prevotella intermedia. Infect Immun 1998;66(12):6054-6057.
16. Iyer D, Anaya-Bergman C, Jones K, Yanamandra S, Sengupta D, Miyazaki H, Lewis JP. AdpC is a Prevotella intermedia 17 leucine-rich repeat internalin-like protein. Infect Immun 2010;78(6):2385-2396.
17. Lamont RJ, Oda D, Persson RE, Persson GR . Interaction of *Porphyromonas gingivalis* with gingival epithelial cells maintained in culture. Oral Microbiol Immunol 1992;7(6):364-367.
18. Socransky SS, Haffajee AD, Cugini MA, Smith C, Kent RL Jr. Microbial complexes in subgingival plaque. J Clin Periodontol 1998;25(2):134-144.

19. Ben Hatit Y, Blum R, Severin C, Maquin M, Jabro MH. The effects of a pulsed Nd:YAG laser on subgingival bacterial flora and on cementum: An *in vivo* study. J Clin Laser Med Surg 1996;14(3):137-143.
20. Chan Y, Chien R. Bactericidal action of Nd:YAG laser radiation in periodontal pockets. In: Loh H-S, editor. 4th International Congress on Lasers in Dentistry, August 6-10, 1994, Singapore. Bologna, Italy: Monduzzi Editore, 1995:Proceedings 4th Int'l Congress on Lasers in Dentistry, Singapore:185-190, 1994.
21. McCawley TK, McCawley MN, Rams TE. LANAP Immediate Effects In Vivo on Human Chronic Periodontitis Microbiota, presented at the American Association for Dental Research annual meeting in March 2014. J Dent Res 2014;93(Spec. Issue A):Abstract 428.
22. Lin PP, Rosen S, Beck FM, Matsue M, Horton JE. A comparative effect of the Nd:YAG laser with root planing on subgingival anaerobes in periodontal pockets. J Dent Res 1992;71(Spec. Issue):299, Abstract 1547.
23. Klinke T, Klimm W, Gutknecht N. Antibacterial effects of Nd:YAG laser irradiation within root canal dentin. J Clin Laser Med Surg 1997;15(1):29-31.
24. Gutknecht N, Fischer J, Conrads G, Lampert F. Bactericidal effects of the Nd:YAG lasers in laser supported curettage. In: Wigdor HA, Featherstone JDB, Rechmann P, editors. Lasers in dentistry III, February 8-9, 1997, San Jose, Calif. Proc. SPIE 2973. Bellingham, Wash.: SPIE – The International Society for Optical Engineering, 1997:221-226.
25. Arany PR. Craniofacial wound healing with photobiomodulation therapy: New insights and current challenges. J Dent Res pii: 0022034516648939. [Epub ahead of print] PMID:27161014
26. Harris DM, JM White, HG Goodis, CJ Arcoria, JS Simon, WM Carpenter, D Fried, J Burkart, M Yessik, T Myers (2002). Selective ablation of surface enamel caries with a pulsed Nd:YAG dental laser. Lasers Surg Med 30:342-350.
27. Harris DM, B McDowell BA, Strisower J. Laser treatment for toenail fungus. In: Kollias N, Choi B, Zeng H, Malek RS, Wong BJ-F, Ilgner JFR, Gregory KW, Tearney GJ, Marcu L, Hirschberg H, Madsen SJ, editors. Photonic therapeutics and diagnostics V, January 22-26, 2009, San Jose, Calif. Proc. SPIE 7161. Bellingham, Wash.: SPIE – The International Society for Optical Engineering, 2009: 71610M-1 – 71610M-7.
28. Harris DM, Yessik M. Therapeutic ratio quantifies laser antisepsis: Ablation of *Porphyromonas gingivalis* with dental lasers. Lasers Surg Med 2004;35(3):206-213.
29. Harris DM, Loomer PM. Ablation of *Porphyromonas gingivalis in vitro* with dental lasers. J Dent Res 2003;82(Spec. Issue):Abstract 855.IADR, San Antonio, March 2003, Poster #855.
30. Harris DM, Jacques SL. Computer simulation of depth of kill of *P gingivalis* in dentin based on experimental damage threshold. Lasers Surg Med 2005;37(Suppl 17):19, Abstract 58.
31. Harris DM. Laser antisepsis of *Phorphyromonas gingivalis in vitro* with dental lasers. In: Rechman P, Fried D, Hennig T, editors. Lasers in dentistry X, January 25, 2004, San Jose, Calif. Proc. SPIE 5313. Bellingham, Wash.: SPIE – The International Society for Optical Engineering, 2004: 91-96.
32. Harris DM, Jacques SL, Darveau R. The black bug myth: Selective photodestruction of pigmented pathogens. Lasers Surg Med 2016; (in press)
33. Shori RK, Walston AA, Stafsudd OM, Fried D, Walsh JT Jr. Quantification and modeling of the dynamic changes in the absorption coefficient of water at λ = 2.94 μm. IEEE J Sel Top Quantum Electron 2001;7(6):959-970.
34. Harris DM, L Reinisch, SL Jacques, R Darveau. Selective destruction of periodontopathogens with dental lasers. Abstr/poster presented at the 101st Annual Meeting of the American Academy of Periodontolog [AAP] Orlando FL, Nov 2015.
35. Berkovitz BKB. Periodontal ligament: Structural and clinical correlates. *Dent Update* 2004;31(1):46-54.

36. Foong K, Sims MR. Blood volume in human bicuspid periodontal ligament determined by electron microscopy. Arch Oral Biol 1999;44(6):465-474.
37. Frank CB. Ligament structure, physiology and function. J Musculoskelet Neuronal Interact 2004;4(2):199-201.
38. Hale, GM, Querry, MR. Optical constants of water in the 200-nm to 200-µm wavelength region. Applied Optics 1973;12(3):555-563.
39. Zijlstra WG, Buursma A, Meeuwsen-van der Roest WP. Absorption spectra of human fetal and adult oxyhemoglobin, de-oxyhemoglobin, carboxyhemoglobin, and methemoglobin. Clinc Chem 1991;37(9):1633-1638.
40. Valvano JW, Cochran JR, Diller KR. Thermal conductivity and diffusivity of biomaterials measured with self-heating thermistors. Int J Thermophys 1985;6(3):301-311.
41. van As G. Erbium lasers in dentistry. Dent Clin North Am 2004;48(4):1017-1059.
42. Onisor I, Pecie R, Chaskelis I, Krejci I. Cutting and coagulation during intraoral soft tissue surgery using Er:YAG laser. Eur J Paediatr Dent 2013;14(2):140-145.
43. Walsh JT Jr, Deutsch TF. Er:YAG laser ablation of tissue: Measurement of ablation rates. Lasers Surg Med 1989;9(4):327-337.
44. Folwaczny M, Aggstaller H, Mehl A, Hickel R. Removal of bacterial endotoxin from root surface with Er:YAG laser. Am J Dent 2003;16(1):3-5.
45. Derdilopoulou FV, Nonhoff J, Neumann K, Kielbassa AM. Microbiological findings after periodontal therapy using curettes, Er:YAG laser, sonic, and ultrasonic scalers. J Clin Periodontol 2007;34(7):588-598.
46. Lopes BMV, Theodoro LH, Melo RF, Thompson GMdA, Marcantonio RAC. Clinical and microbiologic follow-up evaluations after non-surgical periodontal treatment with erbium:YAG laser and scaling and root planing. J Periodontol 2010;81(5):682-691.
47. Akiyama F, Aoki A, Miura-Uchiyama M, Sasaki KM, Ichinose S, Umeda M, Ishikawa I, Izumi Y. In vitro studies of the ablation mechanism of periodontopathic bacteria and decontamination effect on periodontally diseased root surfaces by erbium:yttrium-aluminum-garnet laser. Lasers Med Sci 2011;26(2):193-204. Erratum in: Lasers Med Sci 2011;26(2):277.
48. Meral G, Tasar F, Kocagöz S, Sener C. Factors affecting the antibacterial effects of Nd:YAG laser *In Vivo.* Lasers Surg Med 2003;32(3):197-202.
49. Anderson RR, Parrish JA. Selective photothermolysis: Precise microsurgery by selective absorption of pulsed radiation. Science 1983;220(4596):524-527.
50. Daly CG, Seymour GJ, Kieser JB, Corbet EF. Histological assessment of periodontally involved cementum. J Clin Periodontol 1982; 9(3):266-274.
51. Walsh JT Jr, Flotte TJ, Anderson RR, Deutsch RF. Pulsed CO_2 laser tissue ablation: Dffect of tissue type and pulse duration on thermal damage. Lasers Surg Med 1988;8(1):108-118.
52. Jacques SL. Ratio of entropy to enthalpy in thermal transitions in biological tissues. J Biomed Opt 2006;11(4), 041108-1 – 041108-7.
53. van As G. The diode laser – Tip selection and initiation of the tip. Dent Today 2011;30(5):152.
54. Lamont RJ, Jenkinson HF. Life below the gum line: Pathogenic mechanisms of *Porphyromonas gingivalis*. Microbiol Mol Biol Rev 1998;62(4):1244-1263.
55. Slots J, Bragd L, Wikström M, Dahlén G. The occurrence of Actinobacillus actinomycetemcomitans, Bacteroides gingivalis and Bacteroides intermedius in destructive periodontal disease in adults. J Clin Periodontol 1986;13(6):570-577.
56. Slots J, Listgarten MA. Bacteroides gingivalis, Bacteroides intermedius and Actinobacillus actinomycetemcomitans in human periodontal diseases. J Clin Periodontol 1988;15(2):85-93.
57. Dzink JL, Socransky SS, Haffajee AD. The predominant cultivable microbiota of active and inactive lesions of destructive periodontal diseases. J Clin Periodontol 1988;15(5):316-323.

58. Dorn BR, Leung K-P, Progulske-Fox A. Invasion of human epithelial cells by Prevotella intermedia. Infect Immun 1998;66(12):6054-6057.
59. Socransky SS, Haffajee AD, Cugini MA, Smith C, Kent RL Jr. Microbial complexes in subgingival plaque. J Clin Periodontol 1998;25(2):134-144.
60. Kadowaki T, Nakayama K, Okamoto K, Abe N, Baba A, Shi Y, Ratnayake DB, Yamamoto K. *Porphyromonas gingivalis* proteinases as virulence determinants in progression of periodontal diseases. J Biochem 2000;128(2):153-159.
61. Leknes KN. The influence of anatomic and iatrogenic root surface characteristics on bacterial colonization and periodontal destruction: A review. J Periodontol 1997;68(6):507-516.
62. Grenier D, Turgeon J. Occurrence and identity of proteolytic bacteria in adult periodontitis. J Periodontal Res 1994;29(5):365-370.
63. Tamura M, Tokuda M, Nagaoka S, Takada H. Lipopolysaccharides of *Bacteroides intermedius* (*Prevotella intermedia*) and Bacteroides (*Porphyromonas gingivalis)* induce interleukin-8 gene expression in human gingival fibroblast cultures. Infect Immun 1992;60(11):4932-4937. Erratum in: Infect Immun 1993;61(1):368.
64. Bainbridge BW, Coats SR, Darveau RP. Porphyromonas gingivalis lipopolysaccharide displays functionally diverse interactions with the innate host defense system. Ann Periodontol 2002;7(1):29-37.
65. Kim S-J, Ha M-S, Choi E-Y, Choi J-I, Choi I-S. Prevotella intermedia lipopolysaccharide stimulates release of nitric oxide by inducing expression of inducible nitric oxide synthase. J Periodontal Res 2004;39(6):424-431.
66. Gursoy UK, Könönen E, Uitto V-J. Prevotella intermedia ATCC 25611 targets host cell lamellipodia in epithelial cell adhesion and invasion. Oral Microbiol Immunol 2009;24(4):304-309.
67. Hajishengallis G. Immune evasion strateties of Porphyromonas gingivalis. J Oral Biosci 2011;53(3):233-240.
68. Singh A, Wyant T, Anaya-Bergman C, Aduse-Opoku J, Brunner J, Laine ML, Curtis MA, Lewis JP. The capsule of Porphyromonas gingivalis leads to a reduction in the host inflammatory response, evasion of phagocytosis, and increase in virulence. Infect Immun 2011;79(11):4533-4542.
69. Potempa M, Potempa J, Kantyka T, Nguyen K-A, Wawrzonek K, Manandhar SP, Popadiak K, Riesbeck K, Eick S, Blom AM. Interpain A, a cysteine proteinase from Prevotella intermedia, inhibits complement by degrading complement factor C3. PLoS Pathog 2009;5(2):e1000316. Erratum in: PLoS Pathog 2009;5(3). doi: 10.1371/annotation/e82f810e-738a-47e5-9295-5a0cc9a0dc6c.
70. Perez F, Rochd T, Lodter J-P, Calas P, Michel G. In vitro study of the penetration of three bacterial strains into root dentine. Oral Surg Oral Med Oral Pathol 1993;76(1):97-103.
71. Giuliana G, Ammatuna P, Pizzo G, Capone F, D'Angelo M. Occurrence of invading bacteria in radicular dentin of periodontally diseased teeth: Microbiologic findings. J Clin Periodontol 1997;24(7):478-485.
72. Nalbandian J. The microscopic pattern of tetracycline fluorescence in the cementum of human teeth. J Biol Buccale 1978; 6(1):27-41.
73. Oberoi SS, Dhingra C, Sharma G, Sardana D. Antibiotics in dental practice: How justified are we. Int Dent J 2015;65(1):4-10.
74. Berutti E, Marini R, Angeretti A. Penetration ability of different irrigants into dentinal tubules. J Endod 1997;23(12):725-727.
75. Becker DE. Drug allergies and implications for dental practice. Anesth Prog 2013 60(4):188-197.
76. Oberoi SS, Dhingra C, Sharma G, Sardana D. Antibiotics in dental practice: How justified are we. Int Dent J 2015;65(1):4-10.
77. Rams TE, Degener JE, van Winkelhoff AJ. Antibiotic resistance in human chronic periodontitis microbiota. J Periodontol 2014; 85(1):160-169.

78. Veloo ACM, Seme K, Raangs E, Rurenga P, Singadji Z, Wekema-Mulder G, van Winkelhoff AJ. Antibiotic susceptibility profiles of oral pathogens. Int J Antimicrob Agents 2012;40(5):450-454.
79. Walker CB. The acquisition of antibiotic resistance ..n the periodontal microflora. Periodontol 2000 1996;10(1):79-88.
80. Lakhssassi N, Elhajoui N, Lodter J-P, Pineill J-L, Sixou M. Antimicrobial susceptibility variation of 50 anaerobic periopathogens in aggressive periodontitis: An interindividual variability study. Oral Microbiol Immunol 2005;20(4):244-252.
81. Rodrigues RMJ, Gonçalves C, Souto R, Feres-Filho EJ, Uzeda M, Colombo APV. Antibiotic resistance profile of the subgingival microbiota following systemic or local tetracycline therapy. J Clin Periodontol 2004;31(6):420-427.
82. Bidault P, Chandad F, Grenier D. Risk of bacterial resistance associated with systemic antibiotic therapy in periodontology. J Can Dent Assoc 2007;73(8):721-725.
83. Salyers AA, Whitt DD. Revenge of the Microbes, How bacterial resistance is undermining the antibiotic miracle. ASM Press, Washington DC 2005.
84. Fegan SE, Steiman HR. Comparative evaluation of the antibacterial effects of intracanal Nd:YAG laser irradiation: An in vitro study. J Endod 1995;21(8):415-417.
85. Schoop U, Kluger W, Moritz A, Nedjelik N, Georgopoulos A, Sperr W. Bactericidal effect of different laser systems in the deep layers of dentin. Lasers Surg Med 2004;35(2):111-116.
86. Schoop U, Kluger W, Dervisbegovic S, Goharkhay K, Wernisch J, Georgopoulos A, Sperr W, Moritz A. Innovative wavelengths in endodontic treatment. Lasers Surg Med 2006;38(6):624-630.
87. Vescovi P, Conti S, Merigo E, Ciociola T, Polonelli L, Manfredi M, Meleti M, Fornaini C, Rocca J-P, Nammour S. In vitro bactericidal effect of Nd:YAG laser on Actiomyces israelii. Lasers Med Sci 2013;28(4):1131-1135.
88. Schultz RJ, Harvey GP, Fernandez-Beros ME, Krishnamurthy S, Rodriguez JE, Cabello F. Bactericidal effects of the neodymium:YAG laser: In vitro study. Lasers Surg Med 1986;6(5):445-448.